Journal of Materials Chemistry A

Accepted Manuscript

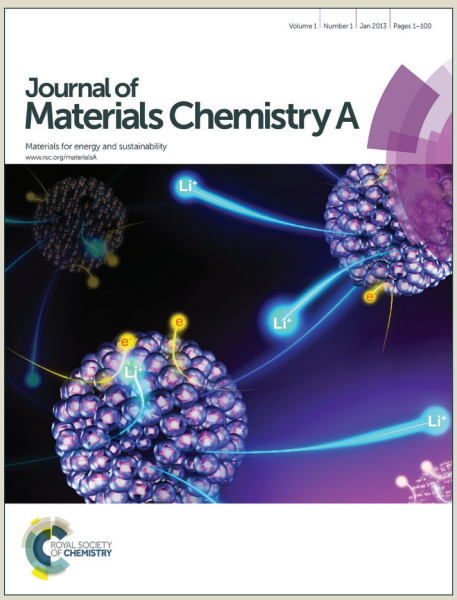

ROYAL SOCIETY OF CHEMISTRY

www.rsc.org/materialsA

Journal of material chemistry A

Dynamic Article Links ►

Cite this: DOI: 10.1039/c0xx00000x

ARTICLE TYPE

www.rsc.org/xxxxxx

High performance polybenzimidazole-CNT hybrid electrode for high-temperature proton exchange membrane fuel cells

He-Yun Du,[a] Chen-Hao Wang,*[b] Chen-Shuan Yang,[b] Hsin-Cheng Hsu,[b] Sun-Tang Chang,[b] Hsin-Chih-Huang,[b] Shiau-Wu Lai,[c] Jyh-Chien Chen,[b] T. Leon Yu,[d] Li-Chyong Chen,[c] Kuei-Hsien Chen*[a,c]

Received (in XXX, XXX) Xth XXXXXXXXX 20XX, Accepted Xth XXXXXXXXX 20XX
DOI: 10.1039/b000000x

Nitrogen-doped CNTs directly grown on carbon cloth (CNT/CC) hybrid with polybenzimidazole are utilized as the hybrid electrode for high-temperature proton exchange membrane fuel cells (HT-PEMFC). Pt nanoparticles (NPs) of typically 2.5 nm in diameter have been deposited uniformly on the electrode composed of either CNT/CC or carbon black on carbon cloth (CB/CC). Comparative study of a 0.1 mg cm^{-2} Pt NPs on PBI-CNT (Pt/PBI-CNT) electrode and a 0.8 mg cm^{-2} Pt NPs on PBI-carbon black (Pt/PBI-CB) for oxygen reduction in the cathode has been performed. In H_2/O_2 HT-PEMFC single cell tests, the low Pt-loading (0.1 mg cm^{-2}) of Pt/PBI-CNT/CC electrode outperform the high Pt-loading (0.8 mg cm^{-2}) of Pt/PBI-CB/CC electrode with maximum power densities of 643 mW cm^{-2} and 468 mW cm^{-2}, respectively, at 160 °C. Notably, the Pt-loading of a Pt/PBI-CNT/CC cell is one eighth of that of Pt/PBI-CB/CC cell, while the former outperforms the latter by approximately 38%. The enhancement is attributed to the good interfacial continuity between PBI membrane and the carbon cloth and the uniform dispersion of the catalyst on the PBI-CNT surface, leading to the formation of three-phase contacts, which is essential for the activity of the catalyst.

Introduction

High-temperature proton exchange membrane fuel cells (HT-PEMFC) that use phosphoric acid-doped polybenzimidazole have become more attractive recently, owing to the increased tolerance of Pt-based hydrogen oxidation catalysts for CO impurities in hydrogen fuel. They can now tolerate up to 2% of such impurities at 180°C. [1-3] Furthermore, HT-PEMFCs offer various advantages, including improved electrode kinetics than low temperature PEMFC, increased efficiency of waste heat utilization, and simplified thermal and water management systems.

PBI is a basic polymer with good thermal and chemical stability, which refers to a group name of heterocyclic polymers that contain benzimidazole units. The PBI is dielectric, but its proton conductivity can be imparted to PBI by adding acid to the polymer film, [4-6] or by direct film casting from PBI solution in polyphosphoric acid. [1, 7, 8] PBI with a high degree of doping with phosphoric acid exhibits excellent proton conductivity at high temperatures, even under anhydrous conditions. Because of the Grotthus mechanism, the operation of HT-PEMFC with a phosphoric acid-doped PBI membrane requires no external humidification of gases. [7] The use of PBI membranes in PEMFC was firstly proposed in various works [4, 9, 10] and many PBI-based membranes have been developed for use in HT-PEMFCs. [2, 11-13] [14-17] However, the use of a PBI membrane that is highly doped with phosphoric acid can result in unfavourable characteristics, including the leaching out of phosphoric acid, poisoning of the Pt catalyst by phosphoric acid and reduced mechanical stability. Accordingly, a high Pt catalyst loading is used in HT-PEMFCs.

Carbon supports, particularly in the form of carbon nanotubes (CNTs), are the highly focused substrate with high electronic conductivity, a large surface area, favourable electrochemical performance and extreme resistance to deterioration under a wide range pH and temperature conditions. [18, 19] Their extraordinary mechanical properties, including a high strength to weight ratio and unique electrical properties that result in high electrical conductivity, have caused material scientists to take much interest in the development of CNTs and their integration into composites to replace inferior materials that would otherwise be utilized. CNT-supported Pt catalysts have been developed for use in low-temperature PEMFCs (< 100 °C), which demonstrate attractive activity, high dispersion, and nano-scale dimensions. [20-23] The idea of utilizing CNT-supported Pt catalysts in HT-PEMFCs has also been demonstrated. [24-27]

In this work, CNTs were directly grown on a carbon cloth, and PBI was loaded onto the CNTs, forming a PBI-CNT hybrid electrode (PBI-CNT). And then the Pt catalysts deposited on PBI-CNT to form a Pt/PBI-CNT electrode as presented in Fig. 1. The interface between Pt catalysts and the PBI-CNT hybrid electrode is carefully controlled with a good phase contact to enable the high performance of HT-PEMFC.

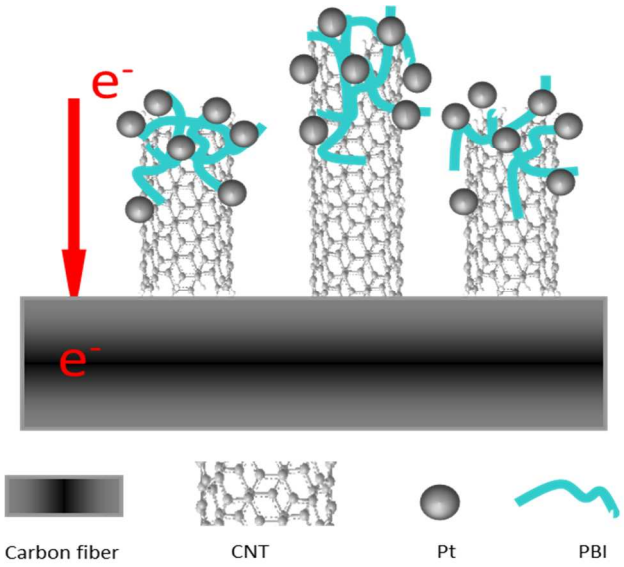

Figure 1. Schematic diagram of the Pt/PBI-CNT on a carbon cloth.

Experimental Section

CNTs were directly and cobalt-assisted catalytically grown on a carbon cloth by the microwave plasma-enhanced chemical vapor deposition method. A sol-gel solution of cobalt (III) nitrate in isopropanol was spread uniformly on the carbon cloth using a spin coater, and was then dried by natural convection. Before CNTs growth, the carbon cloth was pre-treated with hydrogen plasma at a microwave power of 1 kW and a chamber pressure of 28 Torr for 10 min., not only to clean the sample surface but also to convert the cobalt catalyst layer into nanoparticles. CNTs were synthesized in mixed precursors ($CH_4/H_2/N_2$: 20/80/80) at a microwave power of 2 kW, a chamber pressure of 40 Torr, and a substrate temperature of 900 ^oC for 10 min. [28]

PBI (1 mg) was dissolved in dimethyl acetamide (DMAc) (20 mg), and the directly grown CNT electrode was immersed in the solution for 60 min to ensure good PBI coverage on the surface of the CNT electrode. The PBI loading and its thickness were controlled by adjusting the concentration of PBI solution. Then, the PBI-CNT electrode was dried at 180 ^oC for two hours to remove excess DMAc. The PBI-CNT electrode was immersed in 10 % phosphoric acid solution for three days at room temperature to achieve doping and proton conductivity enhancement of the PBI in the PBI-CNT electrode.

In order to prepare the catalyst layer on PBI-CNT, physical vapor deposition (PVD) was used to sputter platinum onto the template to form Pt/PBI-CNT. 24 The platinum target was placed in a radio-frequency planar magnetron sputtering gun in a PVD system. The deposition was conducted in an atmosphere of argon at a working pressure of 5×10^{-2} Torr to yield a highly uniform the CNT-grown carbon paper was 0.1 mg cm^{-2}, which was determined by inductively coupled plasma-optical emission spectroscopy (ICP-OES) analysis.

High-resolution scanning electron microscopy (HRSEM, JEOL-6700F) was utilized to elucidate the micro-structured surface morphologies of the CNTs and the Pt/PBI-CNT. Backscattering electron images were obtained using an r-filter accessory. Transmission electron microscopy (TEM, JEOL-2000FX) was employed to obtain images of CNTs and the Pt catalysts that were loaded on them). The weight per unit area of the metal loading was determined by ICP-OES (Perkin-Elmer ICP-OES Optima 3000). The crystalline structure of the electrocatalysts was examined using an X-ray diffraction (XRD Bruker D8 advance diffractometer system with Cu Kα radiation at 1.54056 Å). FTIR results were analyzed by a Thermo Nicolet Nexus 6700 FTIR spectrograph. Electrochemical measurements were made in a three-electrode test cell at room temperature using a Solartron electrochemical test system (SI 1287). The sample was placed in a specific holder as a working electrode, which was connected to the test system with a gold wire. The reference electrode was a saturated calomel electrode and the counter electrode was platinum foil. All solutions were degassed using high-purity nitrogen and cyclic voltammetry (CV) data were recorded until the CV scans became steady.

The membrane-electrode-assemblies (MEAs) were tested on a 5 cm^2 single cell, with Pt/PBI-CNT as the cathode. For comparison, 0.8 mg cm^{-2} Pt mixed with 1.2 mg cm^{-2} (Johnson Matthew, 40% Pt) and 0.8 mg PBI were loaded on the conventional micro-porous layer using carbon black (E-tek) that had been mixed with 30 wt.% PTFE (Pt/CB) as the cathode. The PBI at catalyst electrode was immersed in 10 % phosphoric acid for three day in order to increase proton conductivity in the electrode. For each MEA, a 0.6 mg cm^{-2} Pt/CB was used as the anode. MEA was fabricated by hot-pressing commercial meta-PBI (Danish power system) that was sandwiched between two electrodes at 145 ^oC and 130 kg cm^{-2} for 5 min.

In the polarization tests, highly pure and unhumidified hydrogen and oxygen both at a flow rate of 200 standard cubic centimeters per minute (SCCM) were fed to the anode and the cathode which were operated at 160 ^oC. A single cell was tested in a PEMFC test station (Asia Pacific Fuel Cell Technologies Ltd.) and the back pressure gauges of both electrodes read 1 atm. The polarization curves were plotted as cell voltage vs. current density in a steady state.

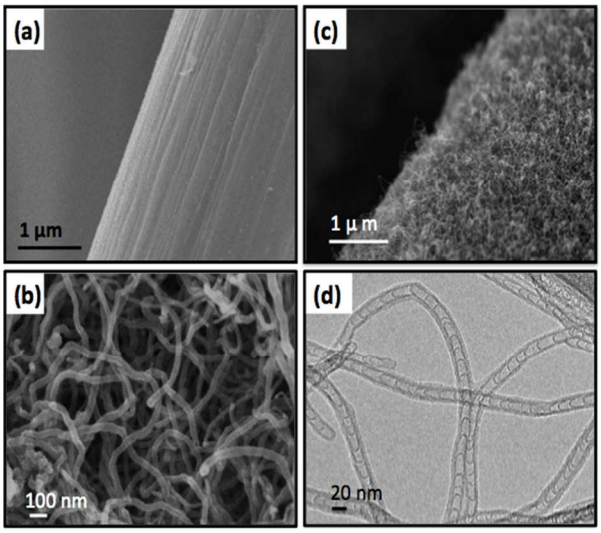

Figure 2. HRSEM images showing (a) carbon fiber of carbon cloth, (b) CNTs directly grown on carbon fiber, and (c) CNT morphology in high magnification; (d) TEM image of bamboo structure CNTs

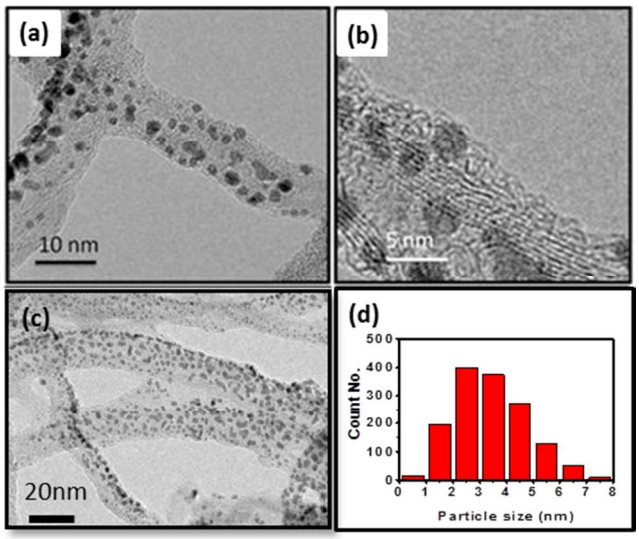

Figure 3. (a) – (c) TEM images of Pt/PBI-CNT in various magnifications; (d) the size histogram of the Pt NPs calculated from Figure 3c.

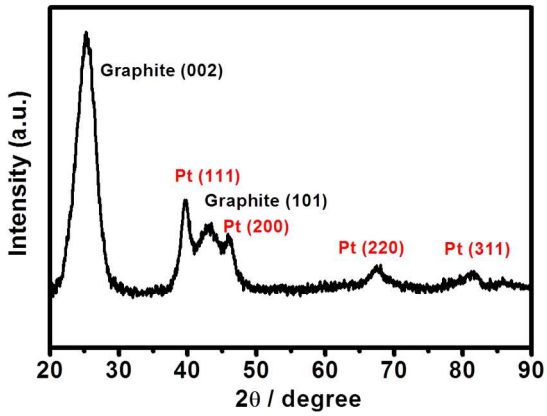

Figure 4. XRD pattern of the Pt/PBI-CNT with representative peaks of Pt and graphite.

Results and Discussion

Figure 2a shows the HRSEM image of the carbon fiber in the carbon cloth. It has a smooth surface and a diameter around 5 μm. Figure 2b presents numerous CNTs that were directly grown on the carbon fiber surface providing a large supporting area for subsequent catalyst deposition. The growth of the CNTs was non-directional and their diameter was approximately 20 nm, as displayed in Fig. 2c. Figure 2d shows the TEM image of typical nitrogen-doped CNTs, which exhibit typical multi-walls and the bamboo-like structure, due to the increased the number of surface defects when nitrogen is incorporated. [29] It's been reported that the nitrogen substitution sites on CNT may function as the initial sites for Pt nucleation during catalyst deposition. [30-32] Figure 3a shows a TEM image of Pt NPs (nano-particles) that are uniformly deposited on a CNT with very few aggregations. Figure 3b presents the morphology of Pt NPs deposited on CNTs that were hybridized with a thin layer of PBI polymer. Here, 5.0 wt.% PBI solution was utilized to form the PBI interlayer between the Pt NPs and the CNT. At the three-phase contact, a Pt catalyst simultaneously establishes three routes for the electrochemical reactions, including a proton conducting route through the PBI, an electron conducting route through CNTs and a gas diffusion route via the pores. Figure 3c shows that Pt NPs are uniformly dispersed CNTs. The small diameter of the Pt NPs provides high catalytic activity attributed to their large surface area. Figure 3d reveals the size distribution of Pt NPs, which have an average diameter of 2.0 – 3.0 nm. The CNTs directly grown on the carbon cloth are inherently beneficial in many aspects. First, its high electrical conductivity provides a highway for the transport of electrons and minimizes the resistive energy loss. Second, the direct connection between CNTs and the carbon cloth substantially reduces the interfacial resistance of the two. Third, the CNTs provide large surface area for the deposition of the Pt NPs, which also reduce the interfacial impedance of the MEA. The hybrid structure of the Pt/PBI-CNT also provides an effective proton-conducting route while allowing gas diffusion to the catalysts.

Figure 4 displays the XRD patterns of the Pt/PBI-CNT. It includes the peaks with 2θ values of 40, 47, 67 and 83°, which are associated with the diffraction of (111), (220), (220) and (311) planes, respectively. The XRD peak for (220) at 68° is isolated from the other carbon diffraction peaks. The grain size can be estimated from this peak using the Scherrer equation:

$$L = \frac{0.9\lambda_{\kappa\alpha 1}}{B_{(2\theta)}\cos\theta_{\max}}, \qquad (1)$$

where B(2θ) is the full width at half maximum. The calculated grain size of the Pt NPs on the PBI-CNT electrode is approximately 3.5 nm, which is consistent with the mean diameter of the Pt NPs that was determine by TEM measurement.

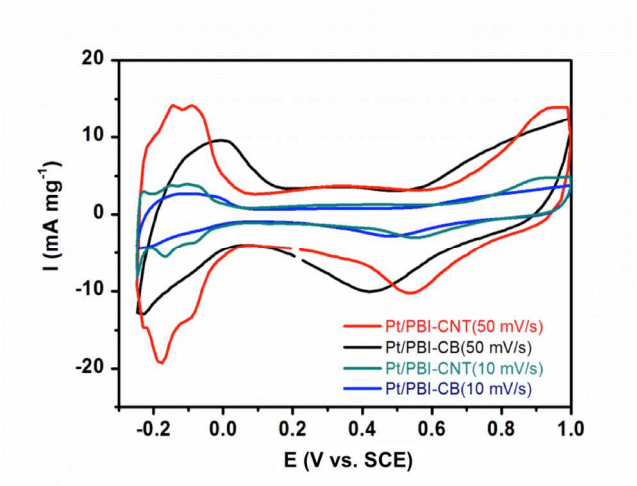

Figure 5. CV measurements for the Pt/PBI-CNT and the Pt/PBI-CB in 0.5 M H_2SO_4 at the scan rates of 10 and 50 mV s^{-1}.

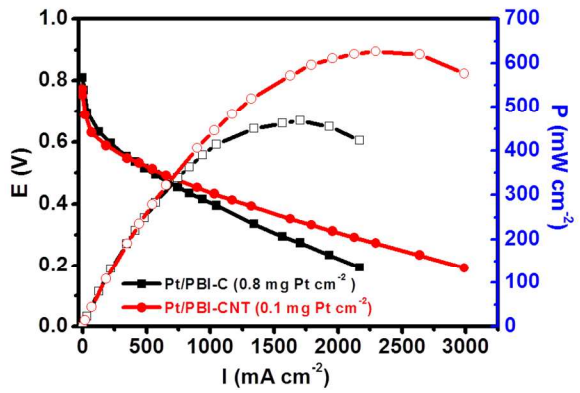

Figure 6. Polarization curves of H_2-O_2 HT-PEMFC using various cathodes operated at 160 ºC with the back pressure of 1 atm.

Table 1. Performances and test condition of different PBI based MEA.

PBI type	Carbon support	Pt loading in cathode (mg/cm^2)	Test conditions	Performance (mW/cm^2)	Ref
m-PBI	N-CNT	0.1	H_2/O_2, 160 □	643	This work
PPQ-pPBI	Carbon black	1	H_2/O_2, 160 □	600	[8]
PBI-SiP	Carbon black	0.5	H_2/O_2, 160 □	480	[15]
PBI	MoOx-CNT	0.25	H_2/O_2, 160 □	360	[24]
PBI	CNT	0.9	H_2/O_2, 150 □	700	[27]
PBI	Carbon black	0.4	H_2/O_2, 170 □	630	[6]
m-PBI	Carbon black	1	H_2/O_2, 160 □	280	[33]
PBI	Carbon black	1	H_2/Air, 160 □	210	[34]

Figure 5 plots the CV curves of the Pt/PBI-CNT and the Pt/PBI-CB in 0.5 M H_2SO_4 solution obtained at the scan rates of 10 and 50 mV s^{-1}. The hydrogen ad/desorption redox peaks of Pt/PBI-CB are shifted to the higher potentials with the higher scan rate, but those of Pt/PBI-CV are fewer changes with the higher scan rate. It indicates that the Pt/PBI-CNT is more reversible than the Pt/PBI-CB, which the former has faster charge-transfer rate than the latter. From the adsorption of protons in the region of hydrogen evolution, the electrochemical surface area (ECSA) of Pt catalysts is given by,

$$ECSA = \frac{|Q_H|}{210\ \mu C}(cm^2), \quad (2)$$

The ECSA provides important information concerning the number of available active sites. It reveals that Pt/PBI-CNT has a higher ECSA (33.4 m^2 g^{-1}) than Pt/PBI-CB (20.5 m^2 g^{-1}) according to the curves at the scan rate of 50 mV s^{-1}. Smaller catalyst particles exhibit greater catalytic activity so the higher ECSA may relate to the fact that Pt NPs are smaller and more uniformly dispersed on the surfaces of CNTs than the CB.

Figure 6 plots the polarization curves of the Pt/PBI-CNT and the Pt/PBI-CB MEA cathodes with metal loadings of 0.1 and 0.8 mg cm^{-2}, yielding maximum power densities of 643 and 468 mW cm^{-2}, respectively. The internal resistance of MEA significantly influences fuel cell performance. The slope of the polarization curve between 0.6 and 0.4 V is associated with the ohmic loss, which is itself determined by the internal resistance, which comprises electronic, ionic and contact resistances. The absolute slope of the curve for Pt /PBI-CNT is much lower than Pt/PBI-CB, revealing that the former has much lower internal resistance. Here, Compared with the maximum power density of various PBI based MEAs, the results are summarized in Table 1. It demonstrates the Pt/PBI-CNT has excellent power density with much lower catalyst amount, which compared with other PBI based MEA.

Conclusions

In summary, Pt/PBI-CNT, in which CNTs are directly grown on carbon cloth before low loadings of Pt catalyst are deposited onto the hybrid structure of the PBI-CNT electrode, was demonstrated for HT-PEMFC applications. The interfacial interaction between Pt NPs and the PBI-CNT electrode reveals a good three-phase contact, a very low electron transfer loss and a contiguous interface layer, resulting in remarkable performance. A maximum power density of 643 mW cm^{-2} has been achieved on a Pt/PBI-CNT MEA cathodes with catalyst loadings of 0.1 mg cm^{-2}, comparative to the 468 mW cm^{-2} on a Pt/PBI-CB MEA cathodes with catalyst loadings 8 times as high. The enhanced performance is attributed to the CNTs in the cathode that provide large surface area and good electrical conductivity of the cathode.

Acknowledgements

The authors would like to thank the Ministry of Education, Academia Sinica, and the National Science Council of Taiwan, for financially supporting this research.

Notes and references

[a] *Institue of Atomic and Molecular Science, Academia Sinica, Taipei, 10617, Taiwan, Fax: +886-2-33665280; Tel:+ 886-2-33665231; E-mail: chenkh@pub.iams.sinica.edu.tw*
[b] *Department of Materials Science and Engineering, National Taiwan University of Science and Technology, Taipei, 10607, Taiwan, Fax: +886-2-27376544; Tel: +886-2-27303715; E-mail: chwang@mail.ntust.edu.tw*
[c] *Center for Condensed Matter Sciences, National Taiwan University, Taipei, 10617, Taiwan*
[d] *Department of Chemical Engineering & Materials Science, Yuan Ze University, Chung-Li, Taoyuan 32003, Taiwan*

Reference

1. G. Qian and B. C. Benicewicz, J. Polym. Sci., Part A-1: Polym. Chem., 2009, **47**, 4064-4073.
2. H. Zhang and P. K. Shen, Chem. Rev., 2012, **112**, 2780-2832.
3. F. Seland, T. Berning, B. Brresen and R. Tunold, J. Power Sources, 2006, **160**, 27-36.
4. J. S. Wainright, J. T. Wang, D. Weng, R. F. Savinell and M. Litt, J. Electrochem. Soc., 1995, **142**, L121-L123.
5. M. Mamlouk and K. Scott, Int. J. Energy Res., 2011, **35**, 507-519.
6. M. Mamlouk and K. Scott, Int. J. Hydrogen Energy, 2010, **35**, 784-793.
7. L. Xiao, H. Zhang, E. Scanlon, L. S. Ramanathan, E.-W. Choe, D. Rogers, T. Apple and B. C. Benicewicz, Chem. Mater., 2005, **17**, 5328-5333.

8. D. C. Seel and B. C. Benicewicz, J. Membr. Sci., 2012, **405-406**, 57-67.
9. J. T. Wang, J. S. Wainright, R. F. Savinell and M. Litt, J. Appl. Electrochem., 1996, **26**, 751-756.
10. J. T. Wang, R. F. Savinell, J. Wainright, M. Litt and H. Yu, Electrochim. Acta, 1996, **41**, 193-197.
11. Q. Li, R. He, J. O. Jensen and N. J. Bjerrum, Fuel Cells, 2004, **4**, 147-159.
12. A. H. Haghighi, M. M. Hasani-Sadrabadi, E. Dashtimoghadam, G. Bahlakeh, S. E. Shakeri, F. S. Majedi, S. Hojjati Emami and H. Moaddel, Int. J. Hydrogen Energy, 2011, **36**, 3688-3696.
13. M. Han, G. Zhang, M. Li, S. Wang, Z. Liu, H. Li, Y. Zhang, D. Xu, J. Wang, J. Ni and H. Na, J. Power Sources, 2011, **196**, 9916-9923.
14. H.-L. Lin, S.-H. Wang, C.-K. Chiu, T. L. Yu, L.-C. Chen, C.-C. Huang, T.-H. Cheng and J.-M. Lin, J. Membr. Sci., 2010, **365**, 114-122.
15. H.-L. Lin, T.-H. Tang, C.-R. Hu and T. L. Yu, J. Power Sources, 2012, **201**, 72-80.
16. H. Xu, K. Chen, X. Guo, J. Fang and J. Yin, polymer, 2007, **48**, 5556-5564.
17. H.-L. Lin, Y.-C. Chou, T. L. Yu and S.-W. Lai, Int. J. Hydrogen Energy, 2012, **37**, 383-392.
18. Q. Lu, B. Yang, L. Zhuang and J. Lu, The Journal of Physical Chemistry B, 2005, **109**, 1715-1722.
19. P. Ajayan and O. Zhou, eds., Applications of Carbon Nanotubes, Springer Berlin / Heidelberg, 2001.
20. Y. Yuan, J. A. Smith, G. Goenaga, D.-J. Liu, Z. Luo and J. Liu, J. Power Sources, 2011, **196**, 6160-6167.
21. P. Hernandez-Fernandez, M. Montiel, P. Ocon, J. L. G. de la Fuente, S. Garcia-Rodriguez, S. Rojas and J. L. G. Fierro, Appl. Catal., B, 2010, **99**, 343-352.
22. N. Rajalakshmi, H. Ryu, M. M. Shaijumon and S. Ramaprabhu, J. Power Sources, 2005, **140**, 250-257.
23. H.-Y. Du, C.-H. Wang, H.-C. Hsu, S.-T. Chang, S.-C. Yen, L.-C. Chen, B. Viswanathan and K.-H. Chen, J. Mater. Chem., 2011.
24. R. Vellacheri, S. M. Unni, S. Nahire, U. K. Kharul and S. Kurungot, Electrochim. Acta, 2010, **55**, 2878-2887.
25. K. Matsumoto, T. Fujigaya, K. Sasaki and N. Nakashima, J. Mater. Chem., 2011, **21**, 1187-1190.
26. M. Lebert, M. Kaempgen, M. Soehn, T. Wirth, S. Roth and N. Nicoloso, Catal. Today, 2009, **143**, 64-68.
27. Suryani, C.-M. Chang, Y.-L. Liu and Y. M. Lee, J. Mater. Chem., 2011, **21**, 7480-7486.
28. C. H. Wang, H. Y. Du, Y. T. Tsai, C. P. Chen, C. J. Huang, L. C. Chen, K. H. Chen and H. C. Shih, J. Power Sources, 2007, **171**, 55-62.
29. L. C. Chen, C. Y. Wen, C. H. Liang, W. K. Hong, K. J. Chen, H. C. Cheng, C. S. Shen, C. T. Wu and K. H. Chen, Adv. Funct. Mater., 2002, **12**, 687-692.
30. C.-H. Wang, H.-C. Shih, Y.-T. Tsai, H.-Y. Du, L.-C. Chen and K.-H. Chen, Electrochim. Acta, 2006, **52**, 1612-1617.
31. H. Y. Du, C. H. Wang, H. C. Hsu, S. T. Chang, U. S. Chen, S. C. Yen, L. C. Chen, H. C. Shih and K. H. Chen, Diamond Relat. Mater., 2008, **17**, 535-541.
32. C.-L. Sun, H.-W. Wang, M. Hayashi, L.-C. Chen and K.-H. Chen, J. Am. Chem. Soc., 2006, **128**, 8368-8369.
33. M. S. Kondratenko, M. O. Gallyamov and A. R. Khokhlov, Int. J. Hydrogen Energy, 2012, **37**, 2596-2602.
34. J. Lobato, P. Cañizares, M. A. Rodrigo, J. J. Linares and F. J. Pinar, Int. J. Hydrogen Energy, 2010, **35**, 1347-1355.